

From Scattering Parameters to Snell's Law: A Subwavelength Near-Infrared Negative-Index Metamaterial

Xuhuai Zhang,¹ Marcelo Davanço,¹ Yaroslav Urzhumov,² Gennady Shvets,² and Stephen R. Forrest^{1,3}

¹*Department of Physics, University of Michigan, Ann Arbor, Michigan 48109-1040, USA*

²*Department of Physics, University of Texas, Austin, Texas 78712-0264, USA*

³*Department of Electrical Engineering and Computer Science, University of Michigan, Ann Arbor, Michigan 48109-2122, USA*

(Received 5 June 2008; revised manuscript received 18 November 2008; published 22 December 2008)

A general relation is derived between the band structure of an arbitrary low-loss unit cell and its effective index of refraction. In addition, we determine the maximum unit cell size that defines the “metamaterial regime” [D. R. Smith *et al.*, Phys. Rev. E **71**, 036617 (2005)]. Furthermore, these general rules allow for the design of a subwavelength near-infrared negative-index material, where the negative refractive index is verified by band calculations to be a bulk property. Full-wavelength simulations of prisms consisting of these unit cells suggest behavior consistent with Snell's law in the negative-index regime.

DOI: 10.1103/PhysRevLett.101.267401

PACS numbers: 78.20.Ci, 73.20.Mf, 75.50.Cc, 78.20.Bh

Engineered metamaterials exhibiting a negative refractive index were first demonstrated in the microwave regime [1], and more recently there have been a number of reports at near-infrared or higher optical frequencies [2]. A negative refractive index should be a bulk property and consistent with Snell's law. However, with the exception of one three-layer structure [3], negative-index materials (NIMs) for use at optical wavelengths [2] consist only of a single layer of unit cells, typically in a “fishnet” structure [4]. Characterization of these structures has generally used the scattering (S) parameter method based on the inversion of their complex transmittance and reflectance [5]. The negative index obtained in this way for optical NIMs may change with an increasing number of layers [3] and, in particular, may reverse its sign [6]. Moreover, this index lacks the physical meaning of refraction [7] if it is not verified by Snell's law, since the S -parameter method assumes that the slab, actually composed of discrete elements, is equivalent to a hypothetical, homogeneous NIM. This assumption is especially questionable in the optical domain, since typical optical NIMs fabricated thus far involve unit cell sizes close to half of the wavelength in at least one dimension [2,8]. With the possible exception of work on surface plasmon polaritons in a waveguide structure [9], no refraction experiment or rigorous first-principle calculations on a fabricated structure has confirmed the presence of a negative refractive index for bulk metamaterials at optical frequencies.

At microwave frequencies, however, negative refraction has been observed in two experiments [10,11], which are considered decisive support to NIMs [12]. These experiments employ prisms made of one-dimensional (1D) NIM unit cells, which exhibit a negative phase index in a particular direction. In those experiments, the incident electromagnetic wave (EMW) propagates within the prism along this direction, so that anisotropy of the unit cell

does not play a role. The EMW is obliquely incident on the hypotenuse from within the prism, and the refracted beam is detected in the far field. Negative refraction occurs due to the negative phase index, i.e., antiparallel energy velocity and wave vector, rather than anisotropy of the material, accompanied by a positive phase index [13]. In Ref. [10], the index determined by the S -parameter method was shown to agree with Snell's law. In Ref. [11], refractive indices measured on two different prisms (i.e., at two different incidence angles) consisting of the same unit cells were shown to be equal.

In this work, we apply photonic band calculations to a near-infrared NIM structure with subwavelength dimensions. The negative index obtained from a monolayer of the structure is verified to be a bulk property. We then derive a general relationship between the band structure of an arbitrary 1D low-loss unit cell and its effective index exhibited in refraction experiments similar to Refs. [10,11]. This relationship confirms the negative index for our structure. Full-wavelength simulations on NIM prisms consisting of our structure show negative refraction consistent with predictions from Snell's law. Finally, the role of the small lateral unit cell size unique to the structure is discussed.

The NIM unit cell is shown in the inset in Fig. 1(a). It consists of 20-nm-thick \times 100-nm-wide Au strips, separated from a 20-nm-thick central continuous Au layer [14] by 15-nm-thick polymer dielectric spacers. The unit cell extends infinitely along the \hat{z} direction and is replicated in both the \hat{x} and \hat{y} directions with a period of 150 nm. These dimensions are consistent with a fabricated structure reported elsewhere [15]. For transverse magnetic (TM)-polarized EMWs propagating along \hat{x} in the x - y plane, i.e., $\mathbf{H} = H_z \hat{z}$, the unit cell is a resonator supporting even and odd- H_z modes with respect to the central plane. Currents flow in opposite (the same) directions along the strips in even (odd) resonance, which is associated with an

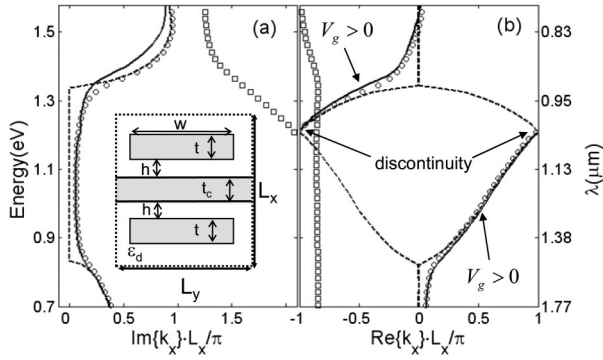


FIG. 1. Bloch bands for zero (dashes) and nonzero dissipation (circles and squares) Au layers, and (a) imaginary and (b) real parts of the effective propagation constant $k_{x,\text{eff}}$ from single-layer scattering simulations (continuous line). In (b), the part of lossless band structure with a positive group velocity $v_g > 0$ is marked by arrows. Inset in (a): The unit cell. Lattice constants $L_x = L_y = 150$ nm, Au strip and central layer thicknesses $t = t_c = 20$ nm, strip width $W = 100$ nm, and spacer thickness $h = 15$ nm. Au strips and central layer are embedded in a polymer dielectric.

effective magnetic (electric) dipole response that is weakly (strongly) dependent on the presence of the central metallic layer [14].

Normal incidence plane wave scattering simulations are performed on a single layer of unit cells to calculate the effective refractive index with the S -parameter method [5]. The refractive index of the polymer dielectric is $n_d = 1.56$ (corresponding to that of cyclotene), and dielectric constants of Au are taken from the literature [16,17]. The index is converted to an effective propagation constant using $k_{x,\text{eff}} = n_{x,\text{eff}}\omega/c = n_{x,\text{eff}}k_0$ and is plotted in Figs. 1(a) and 1(b). Here ω is the angular frequency, c is the speed of light, and k_0 is the wave number in free space. These propagation constants coincide with those derived from Bloch-band calculations (circles and squares) within the first Brillouin zone [18]. Despite the existence of two bands within the same wavelength range, only the least lossy mode (circles, with the smallest $\text{Im}[k_x]$) participates in EMW propagation in the crystal [19]. This coincidence shows that, for a beam traversing a slab containing a sufficiently large number of layers of the structure, the phase delay due to the slab thickness of d can be asymptotically written as $\text{Re}(k_{x,\text{eff}})d = \text{Re}(n_{x,\text{eff}})k_0d$, since phase changes due to the surfaces and possible truncation of the surface unit cells are bounded and hence can be omitted, and multiple reflection amplitudes are negligibly small for any finite $\text{Im}(k_{x,\text{eff}})$. This index is independent of d and is therefore indeed a bulk property.

The Bloch-band diagram for the unit cell assuming lossless Au (i.e., with zero imaginary permittivity) is also plotted in Figs. 1(a) and 1(b) as dashed lines. The band shown by squares has even less contribution to EMW propagation than in the lossy case due to its large imagi-

nary part and is therefore omitted. The Bloch wave vector is real between $\lambda = 0.93$ and $1.5 \mu\text{m}$, a range in which the dimensions of the unit cell are subwavelength ($\sim \lambda/7$). This hypothetical NIM also has both positive- and negative-index bands.

In Fig. 1(b), the discontinuity in $\text{Re}(k_{x,\text{eff}})$ at $\lambda \approx 1 \mu\text{m}$ leads to a discontinuity in $\text{Re}(n_{x,\text{eff}})$. The negative and positive index bands separated by this discontinuity correspond to negative and positive refraction, respectively [10,11]. Consider a two-dimensional semi-infinite metamaterial crystal in the x - y plane composed of these unit cells, as shown in Fig. 2(a). The unit cells are made from dielectric and lossless metal, such that the energy and group velocities of propagating Bloch modes are equal [20]. Furthermore, we assume a TM-polarized Bloch mode propagating along \hat{x} , with wave vector \vec{k} in the first Brillouin zone obliquely incident at the metamaterial-air interface. These modes therefore correspond to the region of the dispersion curves with a positive group velocity, as shown in Fig. 1(b). Because of the finite size of the unit cell, the metamaterial-air interface is stepped, with angle $\theta = \arcsin(a/d) = \arcsin(1/\sqrt{1+m^2})$. Here a is the NIM lattice constant, $d = \sqrt{1+m^2}a$ is the interface periodicity, and there are one and m unit cells along \hat{x} and \hat{y} per step, respectively, as previously [10,11,21]. The resulting interface grating scatters the incident Bloch wave into the transmitted waves.

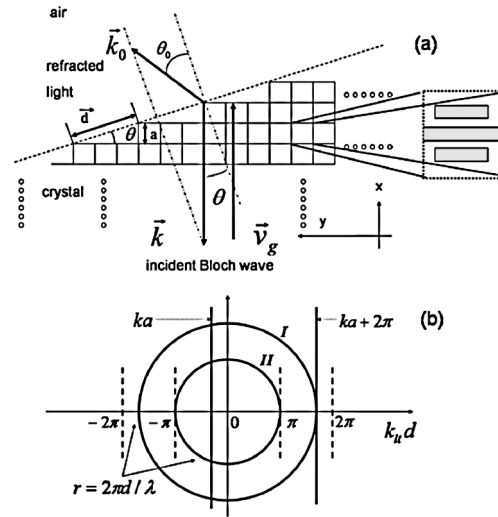


FIG. 2. (a) A Bloch wave propagates in the positive \hat{x} direction and is obliquely incident upon the semi-infinite metamaterial crystal interface with air. Only a small number of unit cells near the interface are shown. Here, a is the lattice constant, and d is the interface periodicity. \vec{k} and \vec{v}_g are the first Brillouin-zone wave vector and group velocity of the incident Bloch wave. \vec{k}_0 is the free space wave vector of the refracted light. θ and θ_0 are incidence and refraction angles, respectively. (b) Graphical solutions to $ka + l \times 2\pi = k_l d$. Radii of circles I and II are $ka + 2\pi$ (for $-\pi < ka < 0$) and π , respectively.

Far from the interface, the scattered optical field can be written as a sum of plane waves following $H(\vec{r}) = \sum_l a_l \exp(i\vec{k}_l \cdot \vec{r})$, where H is the magnetic field, \vec{k}_l is the free space wave vector ($|k_l| = 2\pi/\lambda$), and a_l is the coefficient for the l th term. The component of \vec{k}_l parallel to the interface is related to that of the incident Bloch wave vector \vec{k} through $k_{ll} = k_t + lG$, where $k_t = k \sin\theta$ and $G = 2\pi/d$ is the magnitude of the surface reciprocal lattice vector. This equation is equivalent to $ka + l \times 2\pi = k_{ll}d$, with graphical solutions shown in Fig. 2(b). Each solution of k_{ll} in Fig. 1(a) with the bottom illuminated by a normally incident TM plane wave. The main lobe of the time-averaged power flow of the transmitted wave determines the direction of the refracted beam, which is used to calculate the effective refractive index based on Snell's law. Wedges defined by $m = 2$ and 3 were simulated, corresponding to incidence angles of 26° and 18° , respectively, as in Ref. [11], which also used square unit cells. Both geometries satisfy the condition that $d < d_c$ throughout the simulated frequency range. A representative field plot on a logarithmic scale is shown in the inset in Fig. 3. In the negative-index band, refraction and diffraction coexist, consistent with experiments in the microwave domain [21]. This is due to the lack of complete discrete translational symmetry for the small wedge and enhanced coupling into the diffracted beam by a stepped interface grating between a positive- and a negative-index material [21]. Apart from the main lobe, in most situations two weak side lobes are also apparent. The width of the illuminated part is four steps for both $m = 2$ and 3 wedges, suggesting that the weak side lobes are similar to secondary maxima observed in multiple-slit diffraction experiments. Both features were also observed in microwave frequency simulations where the NIM prism was of a homogeneous composition [21]. A sufficiently large prism eliminates finite size effects such as side lobes and a diffracted beam. Furthermore, the refracted beam would emerge uniformly along the hypotenuse, as shown analytically.

$$n_{\text{eff}} = v_g k / |v_g| k_0 = \frac{\partial \omega}{\partial \text{Re}(k)} k \Big/ \left| \frac{\partial \omega}{\partial \text{Re}(k)} \right| k_0. \quad (1)$$

Figure 1(b) therefore shows that a sufficiently large prism consisting of our (lossless) NIM will undergo negative refraction in the negative-index band of $0.93 \mu\text{m} < \lambda < 1.03 \mu\text{m}$.

Equation (1) connects the first Brillouin-zone band structure of a 1D lossless subwavelength unit cell to its effective index exhibited in a prism refraction experiment. Although its derivation is for TM polarization and the unit cell of Fig. 1, we emphasize that it is general since it utilizes only the discrete translational symmetry along the metamaterial-air interface. This also shows that the stepped interface can be linearized with partial unit cells on the boundary to preserve its discrete translational symmetry. The generalization of the analysis to arbitrary polarization and a 3D subwavelength unit cell is straightforward, provided it has a dominant Bloch band in the incidence direction.

The justification for applying effective medium theory to metamaterials in the literature is that the unit cell size must be much smaller than the wavelength. However, for all NIMs fabricated to date, typically $\lambda/a < 12$ [8]. At the same time, while effective medium theory applies only in the limit $ka \rightarrow 0$, for practical metamaterials $|ka| \sim 1$, a scale that Smith *et al.* refer to as the “metamaterial regime” [22]. Hence, d_c and d_s are quantitative limits based

on physical equivalence that define such a metamaterial regime for 1D NIMs in refraction experiments. These limits and Eq. (1) serve as criteria for the design of NIM unit cells.

A practical structure must be low-loss, for which the above results are also expected to apply. Indeed, the small differences in Figs. 1(a) and 1(b) between the band structure of the lossless and the realistic NIM imply that Eq. (1) is still true for the latter. To confirm this, we performed full-wave simulations of wedges composed of the unit cells in Fig. 1(a) with the bottom illuminated by a normally incident TM plane wave. The main lobe of the time-averaged power flow of the transmitted wave determines the direction of the refracted beam, which is used to calculate the effective refractive index based on Snell's law. Wedges defined by $m = 2$ and 3 were simulated, corresponding to incidence angles of 26° and 18° , respectively, as in Ref. [11], which also used square unit cells. Both geometries satisfy the condition that $d < d_c$ throughout the simulated frequency range. A representative field plot on a logarithmic scale is shown in the inset in Fig. 3. In the negative-index band, refraction and diffraction coexist, consistent with experiments in the microwave domain [21]. This is due to the lack of complete discrete translational symmetry for the small wedge and enhanced coupling into the diffracted beam by a stepped interface grating between a positive- and a negative-index material [21]. Apart from the main lobe, in most situations two weak side lobes are also apparent. The width of the illuminated part is four steps for both $m = 2$ and 3 wedges, suggesting that the weak side lobes are similar to secondary maxima observed in multiple-slit diffraction experiments. Both features were also observed in microwave frequency simulations where the NIM prism was of a homogeneous composition [21]. A sufficiently large prism eliminates finite size effects such as side lobes and a diffracted beam. Furthermore, the refracted beam would emerge uniformly along the hypotenuse, as shown analytically.

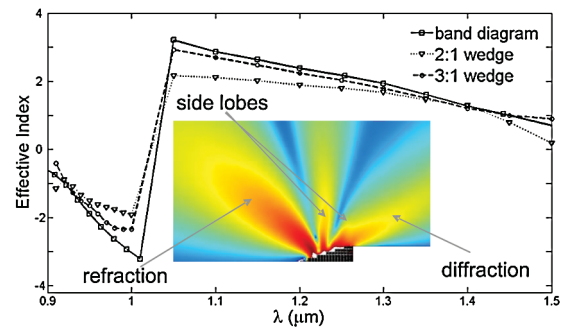


FIG. 3 (color). Comparison of effective indices extracted from numerical simulations and band calculations. Inset: Time-averaged power flow on a logarithmic scale for an $m = 3$ wedge at wavelength $\lambda = 950 \text{ nm}$. A negatively refracted beam, a diffraction order, and two weak side lobes are observed.

Between $\lambda = 0.91$ and $1.5 \mu\text{m}$, refractive indices extracted from the full-wavelength simulations and band structure are plotted in Fig. 3, which are consistent with each other. Since the analytical derivation is rigorous only for a sufficiently large prism, errors are expected for the small wedge considered here. Moreover, the saturation of the $m = 2$ wedge index (triangles) at $n = \pm 2$ for $0.96 \mu\text{m} < \lambda < 1.2 \mu\text{m}$ results since the Bloch-band derived index in this range exceeds the condition for total internal reflection defined by $|n_{\text{max}}| = 1/\sin 26^\circ = 2.2$.

Finally, we discuss the role of unit cell size in transverse dimensions. A homogeneous NIM prism gives rise to no more than one propagating order in air at all incidence angles. To justify the characterization of a NIM structure with a negative index, the refractive behavior of a composite NIM prism made of such unit cells should be consistent with that of a homogeneous NIM prism within the negative-index band in an incidence angle range as large as possible, which was shown to be limited by d_c and d_s . Optical NIMs demonstrated to date typically have lateral dimensions close to $\lambda/2$ [2]. In particular, the lateral unit cell sizes for fishnet structures are constrained by its high magnetic resonance frequency [8,23]. The longitudinal period of a fishnet structure can be very small compared to λ [3], and the incidence angle can be varied almost continuously by changing the number of unit cells in this direction. However, given that the negative index is necessarily strongly dispersive and $|ka|$ is often on the order of unity [22], the maximum incidence angle for a fishnet structure is restricted by its large transverse dimensions. Our unit cell has smaller (i.e., subwavelength) dimensions in the transverse directions where there are field variations, and this restriction is therefore considerably loosened. Hence, for applications requiring a large incidence angle, this type of unit cell is more desirable.

In conclusion, the condition that must be met to observe negative refraction on a prism composed of subwavelength 1D low-loss NIM unit cells is a dominant Bloch band that exhibits an oppositely directed wave vector and group velocity within the first Brillouin zone. The effective index is given by $n_{\text{eff}} = (k/k_0)\text{sgn}[\partial\omega/\partial\text{Re}(k)]$. Such a near-infrared NIM design is presented with realistic material parameters. The geometrical parameters are compatible with a layer-by-layer approach for building a bulk metamaterial [24].

The authors are grateful for discussions with Professors Anthony Grbic and Roberto Merlin. We also thank AFOSR

MURI Contract No. FA 9550-06-01-0279 for financial support.

Note added.—Recently, experimental work [25] using the fishnet structure at a wavelength of $1.5 \mu\text{m}$ was published, where the relation between the band structure and the effective index is consistent with Eq. (1).

-
- [1] D. R. Smith *et al.*, Phys. Rev. Lett. **84**, 4184 (2000).
 - [2] For a complete list of references before 2007, see V. M. Shalaev, Nat. Photon. **1**, 41 (2007); C. M. Soukoulis, S. Linden, and M. Wegener, Science **315**, 47 (2007); U. K. Chettiar *et al.*, Opt. Lett. **32**, 1671 (2007); G. Dolling *et al.*, Opt. Lett. **32**, 53 (2007).
 - [3] G. Dolling, M. Wegener, and S. Linden, Opt. Lett. **32**, 551 (2007).
 - [4] S. Zhang *et al.*, Opt. Express **13**, 4922 (2005).
 - [5] D. R. Smith *et al.*, Phys. Rev. B **65**, 195104 (2002).
 - [6] C. Rockstuhl *et al.*, Phys. Rev. B **77**, 035126 (2008).
 - [7] T. Koschny *et al.*, Phys. Rev. B **71**, 245105 (2005).
 - [8] C. M. Soukoulis *et al.*, J. Phys. Condens. Matter **20**, 304217 (2008).
 - [9] H. J. Lezec, J. A. Dionne, and H. A. Atwater, Science **316**, 430 (2007).
 - [10] C. G. Parazzoli *et al.*, Phys. Rev. Lett. **90**, 107401 (2003).
 - [11] A. A. Houck, J. B. Brock, and I. L. Chuang, Phys. Rev. Lett. **90**, 137401 (2003).
 - [12] J. Pendry, Nature (London) **423**, 22 (2003).
 - [13] J. Yao *et al.*, Science **321**, 930 (2008).
 - [14] V. Lomakin *et al.*, Opt. Express **14**, 11 164 (2006).
 - [15] M. Davanço *et al.*, in *Proceedings of the 20th Annual Meeting of the IEEE, Lasers and Electro-Optics Society, 2007* (IEEE, New York, 2007), p. 325.
 - [16] E. D. Palik, *Handbook of Optical Constants of Solids* (Academic Press, Orlando, 1985).
 - [17] See EPAPS Document No. E-PRLTAO-102-072901 for optical constants of gold used. For more information on EPAPS, see <http://www.aip.org/pubservs/epaps.html>.
 - [18] M. Davanço, Y. Urzhumov, and G. Shvets, Opt. Express **15**, 9681 (2007).
 - [19] D. Seetharamdoo *et al.*, J. Appl. Phys. **98**, 063505 (2005).
 - [20] P. Yeh, J. Opt. Soc. Am. **69**, 742 (1979).
 - [21] D. R. Smith *et al.*, Phys. Rev. Lett. **93**, 137405 (2004).
 - [22] D. R. Smith *et al.*, Phys. Rev. E **71**, 036617 (2005).
 - [23] A. Mary *et al.*, Phys. Rev. Lett. **101**, 103902 (2008).
 - [24] N. Liu *et al.*, Nature Mater. **7**, 31 (2008).
 - [25] J. Valentine *et al.*, Nature (London) **455**, 376 (2008).